Physica B 406 (2011) 430–434

Contents lists available at ScienceDirect

Physica B

journal homepage: www.elsevier.com/locate/physb

The anomalous acoustoelectric current in single-electron transport devices with three pairs of shallow-etched gates

L.B. Liu [a], J. Gao [a,b,*], H.Z. Guo [a], W. Zhang [a], J.H. He [a]

[a] Laboratory of Mesoscopic and Low Dimensional Physics, College of Physical Science and Technology, Sichuan University, Chengdu 610064, PR China
[b] National Institute of Measurement and Testing Technology, Chengdu 610021, PR China

ARTICLE INFO

Article history:
Received 8 July 2010
Received in revised form
30 September 2010
Accepted 3 November 2010

Keywords:
Single electron devices
Acoustoelectric effects
Electron density

ABSTRACT

In order to study the influence of the modulation effect in systems of multiple etched gates, we design single-electron transport devices in an AlGaAs/GaAs heterostructure with three pairs of shallow-etched gates in series. In the experiment, the voltage applied to V_{g1} is set in the pinched-off region; V_{g2} is set in open region and V_{g3} is swept from the pinched-off region to the open. Interestingly, the results indicate that the acoustoelectric current increases from zero to a maximum and then decreases to the zero again, a sharp peak is observed. Change of the electron reservoir's chemical potential is considered as the physical origin of this experimental phenomenon.

1. Introduction

In recent years, surface acoustic wave (SAW) has been employed to drive electrons across the quasi-one-dimensional quantum channels defined by split gate technique [1–6] or shallow-etched gate technique [7–10] in an AlGaAs/GaAs heterostructure. Along the SAW propagating direction, a traveling electric potential is generated. The superposition between the static potential induced by the gates and the traveling electric potential produces a series of moving quantum dots (QDs). Electrons are captured by the SAW-induced QDs at the entrance of quasi-one-dimensional channel and transferred through the channel together with the QDs. A fixed number of the electrons can be transported through the potential barrier due to the electron–electron Coulomb repulsion effect in the dynamic QDs, thus a quantized acoustoelectric (AE) current is produced, $I=nef$, here e is the electron charge; f the SAW frequency; and n an integer.

The significance of this discovery is a possible means of producing a standard of electrical current [11] or a dynamic quantum processor [12,13]. Nevertheless, the exact mechanism of the current quantization has not been fully understood and its application is thus limited. Our experimental result shows an abnormal phenomenon of a triangular-shaped peak, which is similar to Ref. [4]. In Ref. [4], a theoretical model given by Robinson and Barnes [14] could explain the physical mechanism of the triangular-shaped peak of the AE current. In their model the number of electrons is determined by the weakest point of barrier or the maximum potential gradient of the transport direction. However, the structures of our devices vary so much compared with that of Kataoka et al.'s [4], thus we argue that the physical mechanism is different. For our SAW-based single-electron-transport (SAW/SET) devices, three couples of shallow-etched gates are placed in series and the separation between each adjacent pair of gates is wide. In our experiment, the middle gate is set open, and the other two sideward gates are set pinched-off. This means that there are a lot of electrons between these two pinched-off regimes. Therefore, we identify that the potential barrier due to two pairs of pinched-off gates are separated by an electron reservoir. In this regime, if the AE current is generated, the electrons should be carried by the SAW through two separate static potentials and captured twice. Many physical models are used to explain the electron capture mechanism [14–19]. However, these classical models are only applied to the depleted channel in the SAW transport direction, so that these cannot be used to explain our experimental phenomenon.

2. Experimental details

Fig. 1(a) is a schematic layout of our SAW/SET device. The device is fabricated in an AlGaAs/GaAs heterostructure with two-dimensional electron gas (2DEG) situated approximately 80 nm below the surface. The mobility and carrier density are 15 $m^2/V\,s$ and $3.9\times10^{15}\,m^{-2}$, respectively, measured in the dark at 77 K. Two aluminum interdigital transducers (IDTs) are deposited 1.16 mm

* Corresponding author at: Laboratory of Mesoscopic and Low Dimensional Physics, College of Physical Science and Technology, Sichuan University, Chengdu 610064, PR China. Tel.: +86 28 85416606; fax: +86 28 85415508.
E-mail address: prof.j.gao@gmail.com (J. Gao).

0921-4526/$ - see front matter © 2010 Elsevier B.V. All rights reserved.
doi:10.1016/j.physb.2010.11.005

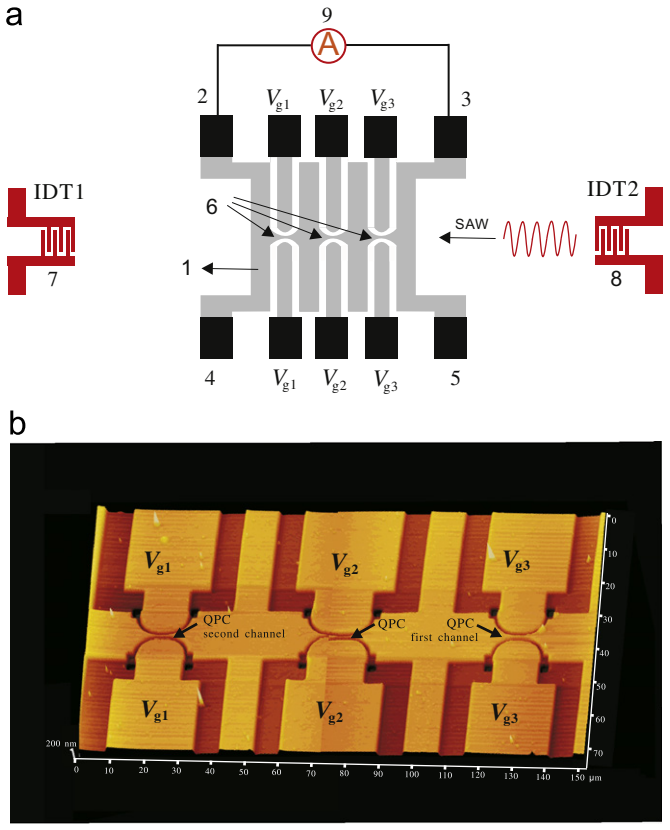

Fig. 1. (a) Schematic diagram of the SAW based single-electron transport device: (1) 2DEG mesa; (2, 3, 4, 5) annealed Au/Ge/Ni alloyed Ohmic contacts; (6) quantum point contacts (QPCs); (7, 8) interdigital transducers (IDTs); (9) ammeter and (b) An atomic force microscopy (AFM) picture of the central region of the QPCs.

apart, on both sides of a 2DEG mesa. The IDT electrode spacing is 2.88 μm thus the SAW center frequency is around 1 GHz. The mesa, contacted with Au/Ge/Ni alloyed Ohmic contacts, is formed in the center of device. Three pairs of etched gates are placed in series in the center of the mesa, as shown in Fig. 1(b). The separation between adjacent gates is 48 μm, and the gate opening for V_{g1}, V_{g2} and V_{g3} are 1.2, 0.5 and 0.8 μm, respectively. Every quantum point contact (QPC) contains two shallow-etched semicircular trenches with radius of 5.5 μm, and a straight segment of 2.8 μm. The trenches etched in our sample are typically 50–60 nm deep and 500 nm wide. Two semicircular shallow-etched trenches form a smooth constriction between the electron reservoirs, whereas the large areas of the 2DEG on both sides of the channel serve as source and drain, respectively.

Our sample is mounted in Oxford refrigerator DR 200 with a base temperature of 10 mK. The measurements are carried out in dc mode at temperature of 0.6 K. All current data is measured by Keithley 6430 sub-Femtoamp Remote Source Meter. The gate voltages are supplied via 18 bit D/A converters NI6289. Radio frequency signals of about 1 GHz is generated by the source Agilent 8648D.

3. Results and discussion

3.1. Quantized acoustoelectric current

Fig. 2 plots a series of the AE current curves, as a function of V_{g3} (swept from the pinched-off region to the open region) under each fixed voltage V_{g1}. The voltage on V_{g1} (fixed in the pinched-off region) increases from −0.9 V (bottom curve) to −0.72 V (top curve) in steps of 0.02 V. V_{g2} is fixed at 2.0 V, the gate is really open. Three pinched-off curves of the gates are shown in insert of Fig. 4. A peculiar feature appeared in Fig. 2 is that the initial current is zero. When V_{g3} is scanned to positive direction, at the beginning the current increases, and reaches a current maximum, then starts to drop until decreases to zero, a sharp peak can be clearly observed. Choosing one of the curves in Fig. 2 for the case of $V_{g1} = -0.76$ V (Fig. 4), the current shows a maximum around $V_{g3} = -1.7$ V. As V_{g3} is swept toward more positive, the current starts to decrease. When $V_{g3} = -1.5$ V, the current eventually decreases to zero and the quantized current plateau appears. The quantized value of the plateau matches that of the original current-quantization plateau (on the left-hand side of the red dotted line, as shown inset of Fig. 2). The red dotted line in Fig. 2 indicates the transition point of V_{g3}. The current on the left of the red dotted line increases quickly while it decreases slowly on the right of the line. This can be simply interpreted as that the influence of the applied voltage on the barrier height is greater when the voltage is more negative [20]. Hence, the left of AE current increases more quickly than that of the right.

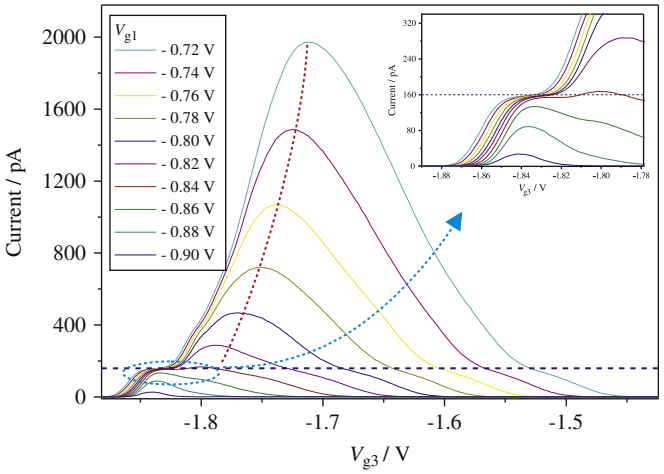

Fig. 2. Acoustoelectric current I with respect to V_{g3}. Different traces are taken at each fixed V_{g1} from −0.72 V (top curve) to −0.9 V (bottom curve) in steps of 0.02 V. Insert: the enlargement of current-quantization plateaux, dashed line indicates the quantized value of the acoustoelectric current (ef=160 pA). V_{g2}=2.0 V, f=1007.45 MHz, P=18.5 dBm, T=0.6 K.

It is known that changing the transducer power has a similar effect on the current–voltage (I–V_{g3}) curve compared with changing V_{g1} [4]. Fig. 3 shows the dependence of acoustoelectric current at different transducer powers. The output power of the signal generator is increased from 15.6 dBm (bottom curve) to 19.2 dBm (top curve) in steps of 0.3 dBm, with the voltages V_{g1} and V_{g2} being fixed at −0.75 and 2.0 V, respectively. Inset in Fig. 3 shows the enlargement of current-quantization plateau, where a dashed line displays the quantized value ef.

3.2. Physical considerations

In the classical model [1], each dynamic QD induced by the SAW captures more than one electron at the entrance of the quasi-one-dimensional channel. As it moves toward the center of the channel, its size decreases, then some electrons leave the dot because of the Coulomb repulsion effect. At fixed SAW power, the static potential barrier is gradually brought down as the gate voltage is swept from negative to positive, which results in a more deep dynamic QD. Hence, more electrons will be captured, and the current increases.

Our experimental results cannot be plausibly explained by the classical model. As V_{g3} is swept to positive, however, the AE current is not always increased. In contrast, the AE current shows a

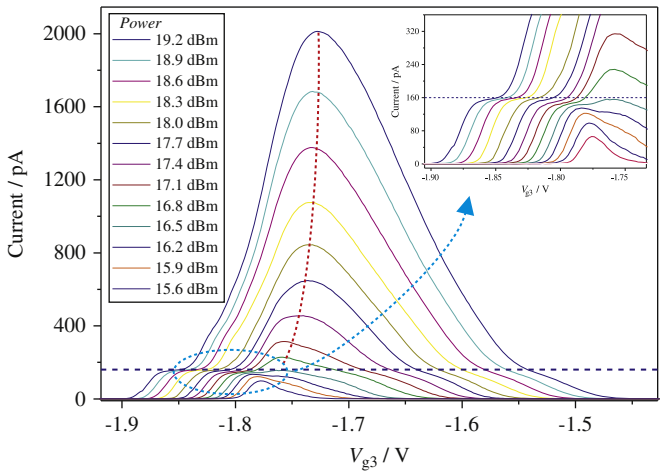

Fig. 3. Acoustoelectric current I as a function of V_{g3} for different SAW powers. The applied SAW powers at the IDT2 increase from 15.6 dBm (bottom curve) to 19.2 dBm (top curve) in steps of 0.3 dBm. Inset shows current-quantization plateaux, dashed line displays the quantized value of the acoustoelectric current. $V_{g1}=-0.75$ V, $V_{g2}=2$ V, $f=1007.45$ MHz, $T=0.6$ K.

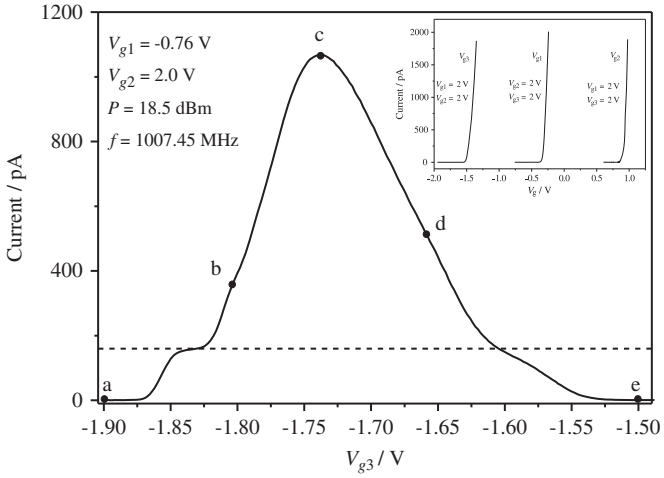

Fig. 4. The experimental curve in Fig. 2 with $V_{g1}=-0.76$ V. Points a, b, c, d, and e mark the voltages corresponding to (a), (b), (c), (d), and (e) in Fig. 5, respectively. Dashed line indicates the quantized value of the acoustoelectric current. Inset shows the three pinched-off curves of V_{g1}, V_{g2} and V_{g3}.

triangular-shaped peak. In our experiment, radio frequency signals are applied to IDT2, as shown in Fig. 1(a). The SAW travels from right to left, so the large areas of the 2DEG on the right of V_{g3} serve as the source and the 2DEG on the left of V_{g1} is drain. The middle gate V_{g2} is set open, and V_{g1}, V_{g3} are set below the pinched-off voltage, that means there are three electron reservoirs in the SAW traveling direction: one on the left of V_{g1}, one between V_{g1} and V_{g3}, another on the right of V_{g3}. If the AE current is produced, at first the electrons should be carried through first channel, then the dynamic QDs will catch the electrons through second channel. In this regime, we present a simple theoretical model to explain the puzzling behavior of a triangular-shaped peak of AE current, as shown in Figs. 2 and 3.

Fig. 4 shows one of the curves in Fig. 2 with $V_{g1}=-0.76$ V, $V_{g2}=2.0$ V. The marked points a, b, c, d, and e are the voltages corresponding to (a), (b), (c), (d), and (e) in Fig. 5, respectively. In our previous work, we have accurately calculated the potential distribution for the split gate structure [20]. However, it is difficult to determine the spatial potential for the shallow-etched structure, because the shape of gate is complex and the surface state in each etched sidewall is difficult to be accurately confirmed [21,22]. For this reason, we can draw a sketch map of the potential distribution along the channel based on the theoretical solution for split gates structure.

Fig. 5(a)–(e) shows the sketch maps of the potential distribution along the channel (SAW traveling direction, from right to left) for five different values of V_{g3}. In Fig. 5(a), when $V_{g3}=-1.9$ V, both potential peaks are very high. As a result, the SAW cannot carry the electrons through both of the channels, and I (measured by our current ammeter), I_1, and I_2 are all equal to zero. When the V_{g3} is set above -1.87 V (Fig. 6), the AE current appears, which means at $f=1007.45$ MHz, $P=18.5$ dBm, the SAW can carry electrons through the static potential produced by $V_{g3}=-1.87$ V. From Fig. 6 we can deduce that a lot of electrons can be carried through first channel from region 1 to region 2. At the case of $V_{g3}=-1.8$ V, the potential distribution is shown in Fig. 5(b). Change in the number of electrons in region 2 is determined by the superposition of the electrons carried by SAW from region 1 to region 2 and the electrons tunneling from region 2 to region 1 (the static potential induced by V_{g1} is much higher than that of V_{g3}, so we only consider tunneling effect from region 2 to region 1). It is believed that regions 1, 2 and 3 have the same chemical potential in the absence of SAW. Moreover, the areas of regions 1, 3 are very larger than that of region 2, therefore, much more electrons are in regions 1 and 3 than that in region 2. Therefore, the μ_1 and μ_3 are considered as a constant. When V_{g3} is equal to -1.8 V the potential is still very high, thus few of electrons can tunnel from region 2 to region 1. On the other hand, lots of electrons are carried by SAW from region 1 to region 2. Hence, the electron density in region 2 will increase, more electrons will occupy higher level and lead to an increase of μ_2 [23]. That will result in a relatively lower potential induced by V_{g1}, thus it is convenient for the SAW to carry the electrons through second channel. Consequently, the AE current is generated. In addition, the height of μ_2 is not always changed. If we fix different voltages on V_{g3}, the change of μ_2 can be done instantaneously. Then I, I_1, and I_2 reach a dynamic equilibrium, and the magnitude of I is equal to I_1 subtracts I_2.

When V_{g3} is swept to a little positive, as shown in Fig. 5(c), the static potential induced by V_{g3} becomes lower. The SAW can carry more electrons through first channel and I_1 will increase. Meanwhile, decrease of the potential induced by V_{g3} will result in more electrons tunnel from region 2 to region 1 and I_2 also increases. However, the growth rate of I_1 is faster than that of I_2, hence more and more electrons are in the region 2 and the μ_2 continues increasing and the chemical potential difference between regions 1 and 2 becomes bigger. The highest μ_2 can be achieved at the moment that the maximal difference between I_1 and I_2. At this time, the SAW carries most electrons through second channel, and I (equal to I_1 subtracts I_2) shows a peak. Corresponding to the peak of the AE current, V_{g3} is swept to more positive values. The static potential induced by V_{g3} becomes very low, thus the μ_2 cannot be maintained at a high level, or else I_2 will be bigger than I_1, the circuit cannot form a steady current. Consequently, more electrons will go back to region 1 again. Both of the electron density and the chemical potential of the region 2 will decrease, as shown in Fig. 5(d). Therefore, it will be more difficult for SAW to carry the electrons through second channel, as a result, I will decrease. In this regime, the sudden transition of the sharp peak in the current arises from a change in the potential of V_{g3}, at one point tries to increase the current and the other tries to decrease it. As V_{g3} is swept in the open-channel regime (the voltage fixed on it is greater than or equal to -1.5 V, according to the insert of Fig. 4), regions 1 and 2 couple with each other, and regions 1–3 have the same chemical

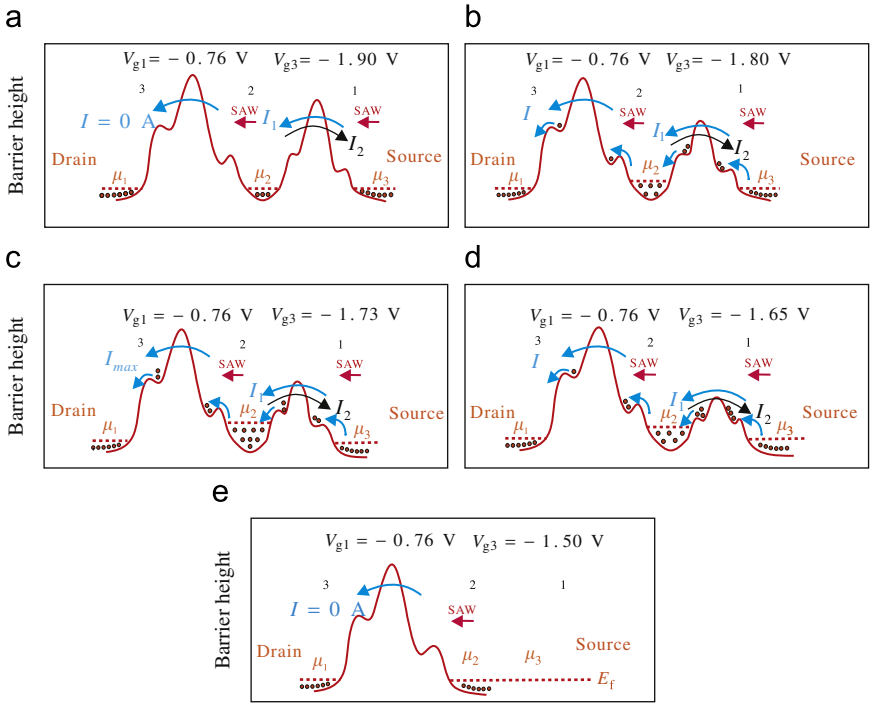

Fig. 5. (a), (b), (c), (d), and (e) show five cases of the schematic diagram of potential height for Fig. 4 in the SAW traveling direction with different V_{g3}: (a) $V_{g3}=-1.9$ V, (b) $V_{g3}=-1.8$ V, (c) $V_{g3}=-1.73$ V, (d) $V_{g3}=-1.65$ V, and (e) $V_{g3}=-1.5$ V, respectively. I displays the equivalent current is produced by QDs caught electrons from region 2 to region 3; I_1 displays the equivalent current is produced by QDs caught electrons from region 1 to region 2; I_2 displays the equivalent current is produced by the electrons tunnel from region 2 to region 1. The μ_1,μ_2 and μ_3 display the chemical potentials of regions 1, 2 and 3, respectively.

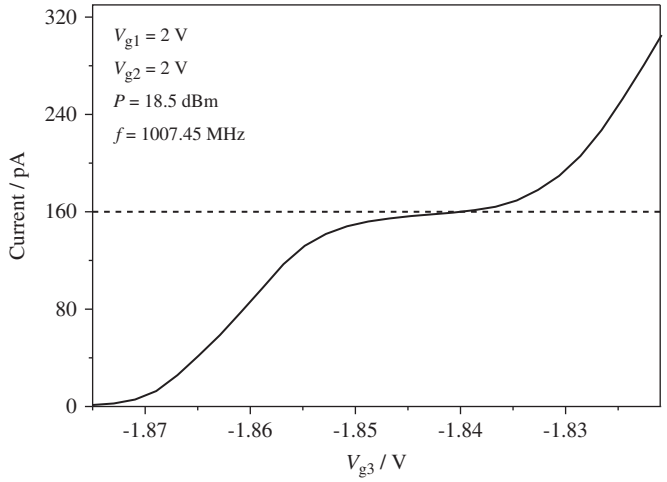

Fig. 6. Theacoustoelectric current as a function of V_{g3} under the following conditions: $V_{g1}=2$ V, $V_{g2}=2$ V, $f=1007.45$ MHz, $P=18.5$ dBm, $T=0.6$ K. The dashed line indicates the quantized value of the acoustoelectric current ($ef=160$ pA).

potential. When $V_{g3}=-1.5$ V the first channel start to open, as shown in Fig. 5(e), region 2 has no regulating effect, and again, no AE current flows.

4. Summary

In summary, we have investigated our SAW/SET devices with three pairs of shallow-etched gates in detail. Experimental result presents a triangular-shaped peak of acoustoelectric current with current-quantization plateaux on both sides. This abnormal behavior can be explained by the change of the electron reservoir's chemical potential. The work also represents that it is possible to modulate acoustoelectric current in systems of micron-separated etched gates.

Acknowledgments

The authors would like to thank for the support of the Key Program of the National Natural Science Foundation of China, under Grant no. 60436010, and the National Key Technology R&D Program of China, under Grant no. 2006BAF06B09.

References

[1] J.M. Shilton, V.I. Talyanskii, M. Pepper, D.A. Ritchie, J.E.F. Frost, C.J.B. Ford, C.G. Smith, G.A.C. Jones, J. Phys. Condens. Matter 8 (1996) L531.
[2] J. Cunningham, V.I. Talyanskii, J.M. Shilton, M. Pepper, M.Y. Simmons, D.A. Ritchie, Phys. Rev. B 60 (1999) 4850.
[3] J. Ebbecke, N.E. Fletcher, T.J.B.M. Janssen, F.J. Ahlers, M. Pepper, H.E. Beere, D.A. Ritchie, Appl. Phys. Lett. 84 (2004) 4319.
[4] M. Kataoka, C.H.W. Barnes, H.E. Beere, D.A. Ritchie, M. Pepper, Phys. Rev. B 74 (2006) 085302.
[5] M.R. Astley, M. Kataoka, C.J.B. Ford, C.H.W. Barnes, D. Anderson, G.A.C. Jones, I. Farrer, D.A. Ritchie, M. Pepper, Phys. Rev. Lett. 99 (2007) 156802.
[6] M.R. Astley, M. Kataoka, C.J.B. Ford, C.H.W. Barnes, M.D. Godfrey, I. Farrer, D.A. Ritchie, D. Anderson, G.A.C. Jones, M. Pepper, S.N. Holmes, J. Appl. Phys. 103 (2008) 096102.
[7] J. Cunningham, V.I. Talyanskii, J.M. Shilton, M. Pepper, A. Kristensen, P.E. Lindelof, Phys. Rev. B 62 (2000) 1564.
[8] K. Gloos, P. Utko, J.B. Hansen, P.E. Lindelof, Phys. Rev. B 70 (2004) 235345.
[9] P. Utko, J.B. Hansen, P.E. Lindelof, C.B. Sørensen, K. Gloos, J. Low. Temp. Phys. 146 (2007) 607.
[10] S.J. Wright, M.D. Blumenthal, M. Pepper, D. Anderson, G.A.C. Jones, C.A. Nicoll, D.A. Ritchie, Phys. Rev. B 80 (2009) 113303.
[11] K. Flensberg, A.A. Odintsov, F. Liefrink, P. Teunissen, Int. J. Mod. Phys. B 13 (1999) 2651.
[12] C.H.W. Barnes, J.M. Shilton, A.M. Robinson, Phys. Rev. B 62 (2000) 8410.

[13] C.H.W. Barnes, Philos. Trans. R. Soc. London A 361 (2003) 1487.
[14] A.M. Robinson, C.H.W. Barnes, Phys. Rev. B 63 (2001) 165418.
[15] P.A. Maksym, Phys. Rev. B 61 (2000) 4727.
[16] G.R. Aĭ zin, G. Gumbs, M. Pepper, Phys. Rev. B 58 (1998) 10589.
[17] G. Gumbs, G.R. Aĭzin, M. Pepper, Phys. Rev. B 60 (1999) R13954.
[18] K. Flensberg, Q. Niu, M. Pustilnik, Phys. Rev. B 60 (1999) R16291.
[19] N.E. Fletcher, J. Ebbecke, T.J.B.M. Janssen, F.J. Ahlers, M. Pepper, H.E. Beere, D.A. Ritchie, Phys. Rev. B 68 (2003) 245310.
[20] H.Z. Guo, J. Gao, C. Lu, J. Appl. Phys. 105 (2009) 124302.
[21] B. Jogai, J. Appl. Phys. 93 (2003) 1631.
[22] C.Y. Zhang, J. Gao, H.Z. Guo, C. Lu, Phys. Lett. A 374 (2010) 1389.
[23] C.W.J. Beenakker, Phys. Rev. B 44 (1991) 1646.